3 DoF Vibration Compensation Platform for Robot-Based Precision Inline Measurements on Free-Form Surfaces

Daniel Wertjanz, Ernst Csencsics, and Georg Schitter, *Senior Membership, IEEE*

***Abstract*—This paper presents a three DoF MAGLEV vibration compensating measurement platform (MP) with arbitrary operation orientation for robot-based surface inspection of free-forms. The MP design comprises an internal position sensor system which is used in feedback control to maintain a free-floating position in six DoFs with respect to its supporting frame when approaching a sample (stabilization mode). In addition, the integrated design includes three tracking sensors measuring the out-of-plane position of the MP to a sample surface. The entire system can be mounted as an end effector of an industrial robot with the MP carrying a desired measurement tool. Disturbing environmental vibrations are actively compensated by maintaining a constant position of the MP with respect to a sample surface (tracking mode). The control design includes SISO position controllers for all DoFs, achieving a bandwidth of about 130 Hz. By means of a cross-fading error gain, an efficient control transition between stabilization and tracking mode is enabled. A vibrating target is used to evaluate the vibration compensation performance of the tracking module for standardized floor vibration profiles. Attenuation between -35 and -20 dB for out-of-plane vibrations below 40 Hz is achieved. In the time domain, vibration profiles with 15.7 µm rms and 95 µrad rms are reduced to 1.6 µm rms and 21 µrad rms, respectively.**

***Index Terms*—Mechatronics, Vibration control, Magnetic levitation.**

I. Introduction

THE assurance of product quality and a continuously growing productivity have become increasingly important in industrial manufacturing in the last decades [1]. Inline measurement systems are consequently regarded as a key factor for future industrial production [2] and are required to be fast, highly precise, versatile, and robust [3]. Frequently, surface properties, such as flatness or roughness, need to be measured on free-formed machined goods together with the deviation from its desired shape [4]. The fields of application range from the automotive to the semiconductor sector [5], [6].

Manuscript received Month xx, 2xxx; revised Month xx, xxxx; accepted Month x, xxxx. The financial support by the Christian Doppler Research Association, the Austrian Federal Ministry for Digital and Economic Affairs, and the National Foundation for Research, Technology and Development, as well as MICRO-EPSILON MESSTECHNIK GmbH & Co. KG and ATENSOR Engineering and Technology Systems GmbH is gratefully acknowledged. The authors are with the Christian Doppler Laboratory for Precision Engineering for Automated In-Line Metrology, Automation and Control Institute (ACIN), Technische Universität Wien, 1040 Vienna. Corresponding author: wertjanz@acin.tuwien.ac.at

However, the operation of a high resolution surface measurement system directly in the vibration prone environment of an industrial production line is considered as a major challenge. Most high precision measurement tools (MTs) need to be properly aligned with respect to the sample surface and are highly vibration sensitive. Environmental vibrations cause motion blur in the measurement results in all degrees of freedom (DoFs) [7], corrupting measurements at the micrometer scale [8] by transmission to the MT and sample via rigid-body connections. Current solutions include passive and active vibration isolation concepts [9], which are mostly spatially separated from the production line, in order to minimize the impact of the industrial environment. Therefore, a 100 % quality control is usually not possibly and the produced goods are inspected only randomly.

The flexibility to measure muliple spots on free-formed surfaces [10] at arbitrary positions in arbitrary orientations is another requirement future measurement systems have to deal with. Industrial robots are an appropriate tool that can be employed for enabling this flexibility [11], but are lacking the required positioning accuracy. By applying feedback control, robot arms achieve an accuracy of 50 µm [12] which is, however, still about two orders of magnitude too low for precision 3D measurements [13]. Recently, a robot-based approach combining the flexibility of a robot arm with a high precision 3D MT has been proposed [14]–[17]. Acting as an end effector, a magnetic levitation (MAGLEV) tracking platform maintains a constant distance between the sample surface and the 3D MT on the platform, by means of feedback control. Thus, a contactless stiff link between sample and MT is established, compensating the influence of environmental vibrations. However, the proposed approach is limited to a single operation orientation of the system, as a result of the implemented permanent magnet assembly for gravity compensation. As a first step towards robot-based precision measurements on free-form surfaces, a six DoF MAGLEV positioning platform with orientation independent performance has been developed [18].

The contribution of this paper is i) the modelling and integration of a tracking module for robot-based measurement applications that is able to position the free-floating measurement platform (MP) in a constant distance and orientation to either a vibrating sample surface or its supporting frame, based on a tailored control scheme, and ii) the experimental evaluation of the system performance in a vibrational environment.

Post-print version of the article: D. Wertjanz, E. Csencsics, and G. Schitter, "3 DoF Vibration Compensation Platform for Robot-Based Precision Inline Measurements on Free-Form Surfaces," *IEEE Transactions on Industrial Electronics*, Early access, 2021. DOI: 10.1109/TIE.2021.3055132

The concept and system design of a vibration compensating tracking module enabling precision robot-based measurements on free-form surfaces is described in Section II. The according system dynamics are modeled in Section III. The prototype system is implemented in Section IV, including the identification of the real system dynamics. Section V presents the control design of the stabilization and tracking mode of the MP as well as the efficient transition scheme between the two operational modes. The system performance is experimentally validated in Section VI by means of a moving target, emulating standardized floor vibrations. Finally, Section VII concludes the paper.

II. Tracking Module Design for Robot-Based Precision Measurements

A. Robot-based precision inline measurement concept

The system concept of robot-based precision inline measurements on free-form surfaces is presented in Fig. 1. A robot arm carrying the tracking module is used to extend the range of a high precision MT and to coarsely align it with respect to a sample surface. A suitable MT with an integrated scanning mechanism, such as presented in [19], [20], to perform 3D surface measurements is mounted on an electromagnetically actuated MP, which is embedded into the supporting frame of the tracking module. Integrated tracking sensors (TS) are used to measure the distance and orientation of the MP with respect to the sample surface z_e, whereas internal position sensors (IPS) measure the MP's position relative to its supporting frame z_i. By means of feedback control, the MP ensures a constant alignment z_e of the MT to the sample surface, establishing a contactless stiff link. Thus, disturbing relative motions between the MT and the sample surface caused by environmental vibrations z_S are actively compensated, forming a vibration-free lab environment directly in a vibration-prone environment and enabling precision 3D surface measurements. Vibrations in industrial workshops are significantly present in the frequency domain below 80 Hz [7]. To attenuate the predominant components of the vibration spectrum with up to 8 Hz by at least a factor of ten (20 dB), a tracking control mode bandwidth greater than 80 Hz is required. For an increasing tracking bandwidth the vibration compensation performance increases as well [21]. Therefore, the tracking control mode bandwidth is targeted to be as high as possible. The targeted tracking range is set to $\pm 100\,\mu$m in the translational DoFs.

B. Tracking module design

The mechatronic design of the tracking module in Fig. 1 comprises an integrated MAGLEV actuation system (AS) based on voice coil actuators (VCAs) to mechanically decouple the moving platform and to achieve quasi-zero-stiffness actuation. Considering the targeted application of robot-based measurements of free-form surfaces, the vibration compensation capability of the platform needs to be independent on the actual robot pose and orientation of the entire measurement module. Therefore, high actuation forces are required to electromagnetically levitate and actuate the platform. Moreover, a lightweight MP design and high precision TS are desirable in order to achieve a good vibration compensation performance.

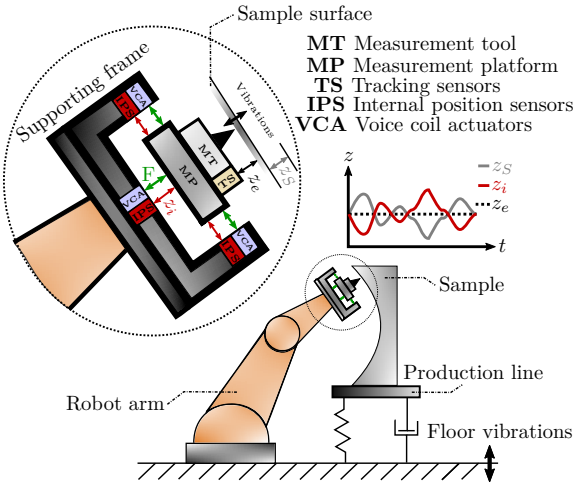

Fig. 1: Multi-DoFs vibration compensation concept for robot-based precision inline surface measurements on free-forms. An electromagnetically actuated tracking system compensates disturbing environmental vibrations by maintaining a constant alignment z_e of the MT with respect to the sample surface.

Figure 2a depicts the design of the tracking module with the support frame and the MP, enabling arbitrary operation orientation. The system design comprises eight identical VCAs A_1-A_8 for a deliberate over-actuation, yielding to a balanced MP design. The capability of providing bi-directional forces and the symmetric placement of the VCAs enable the desired orientation-independent system operability. To achieve a lightweight MP design, the coils of the VCAs are mounted on the MP, which is actuated within the air gaps between coils and magnet assemblies of the VCAs. Hence, the actuator placement significantly determines the achievable actuation range. A_5-A_8 enable in-plane positioning (x_i, y_i and $\phi_{z,i}$) of the mover, while the out-of-plane DoFs z_i, $\phi_{x,i}$ and $\phi_{y,i}$ are actuated by A_1-A_4. The actuators are symmetrically placed beneath and around the moving MP. To avoid unintended torsional motion through actuation and aiming for a good decoupling between all DoFs, the actuators A_5-A_8 are placed on the same height as the MP's center of mass on the z-axis (Fig. 2b). Regarding the actuator placement in the xy-plane, high levers of torque for the rotational DoFs are desirable to provide high torsional forces. However, the realizable actuation range decreases with increasing lateral displacement of the actuators. Therefore, a trade-off between achievable actuation range and levers of torque is made with resulting design parameters shown in Section IV. An IPS system determines the MP position in all DoF with respect to the supporting frame. IPS_1-IPS_3 are placed beneath the MP and detect the out-of-plane position, whereas the sensors IPS_4-IPS_6 are mounted around the MP and measure the in-plane position.

In order to enable active vibration compensation in the three

Post-print version of the article: D. Wertjanz, E. Csencsics, and G. Schitter, "3 DoF Vibration Compensation Platform for Robot-Based Precision Inline Measurements on Free-Form Surfaces," *IEEE Transactions on Industrial Electronics*, Early access, 2021. DOI: 10.1109/TIE.2021.3055132

out-of-plane DoFs, the external out-of-plane position of the MP relative to a sample surface (z_e, $\phi_{x,e}$ and $\phi_{y,e}$) is measured by a set of three tracking sensors TS_1-TS_3 as illustrated in Figure 2b. The TS are mounted on the MP and on the same axes as the out-of-plane IPS.

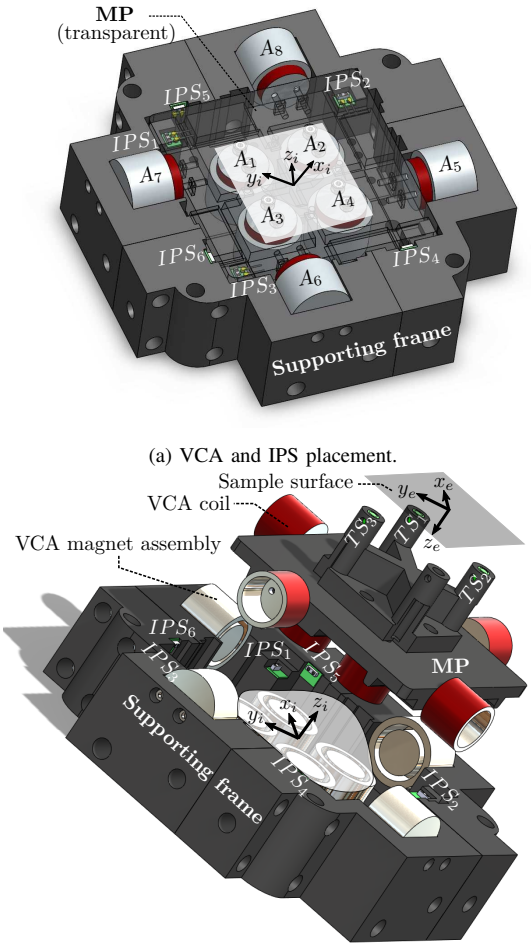

(a) VCA and IPS placement.

(b) Exploded view of tracking platform prototype.

Fig. 2: Design of the multi-DoF vibration compensation module. a) VCAs are used to actuate the platform in six DoFs. IPS determine the platform position with respect to the supporting frame. b) A set of three TS enables the measurement of the out-of-plane position and orientation relative to a sample surface.

III. System Modeling

A decoupled actuation between the out-of-plane (A_1-A_4) and in-plane DoFs (A_5-A_8) is achieved by the VCA placement in Fig. 2b, yielding a balanced MP design. Based on the system design, low cross talk between the individual DoFs is expected and therefore neglected in the modeling phase. The cross talk, however, is analyzed later in Section IV-B. To levitate the MP, the gravitational force needs to be compensated in arbitrary orientations. Since the MP is freely floating, friction-free and quasi-zero-stiffness actuation is ensured by operating the hysteresis-free VCAs around the mid-position, yielding a constant force to current relation [13], [22]. Assuming a floating mass model, the MP dynamics using the coordinate system of the internal position $\boldsymbol{\zeta}_\mathbf{i}$ can be written in state-space representation as

$$\ddot{\boldsymbol{\zeta}}_\mathbf{i} = \begin{bmatrix} \ddot{\boldsymbol{\zeta}}_{\mathbf{i,oop}} \\ \ddot{\boldsymbol{\zeta}}_{\mathbf{i,ip}} \end{bmatrix} = \mathbf{A}\mathbf{i} = \begin{bmatrix} \mathbf{A_{oop}} & \mathbf{0_{3,3}} \\ \mathbf{0_{3,3}} & \mathbf{A_{ip}} \end{bmatrix} \begin{bmatrix} \mathbf{i_{oop}} \\ \mathbf{i_{ip}} \end{bmatrix} \tag{1}$$

with $\boldsymbol{\zeta}_{\mathbf{i,oop}} = \begin{bmatrix} z_i & \phi_{x,i} & \phi_{x,i} \end{bmatrix}^T$ and $\boldsymbol{\zeta}_{\mathbf{i,ip}} = \begin{bmatrix} x_i & y_i & \phi_{z,i} \end{bmatrix}^T$ being the out-of-plane and in-plane MP position measured by the IPS, respectively. $\mathbf{A_{oop}}$ and $\mathbf{A_{ip}}$ denote the according dynamic matrices, and the electrical current vectors are $\mathbf{i_{oop}} = \begin{bmatrix} i_z & i_{\phi_x} & i_{\phi_y} \end{bmatrix}^T$ and $\mathbf{i_{ip}} = \begin{bmatrix} i_x & i_y & i_{\phi_z} \end{bmatrix}^T$. Considering the actuator placement and the chosen coordinate systems in Fig. 2b, the dynamic matrix $\mathbf{A}$ is given by

$$\mathbf{A} = \begin{bmatrix} \frac{4k_m}{m} & 0 & 0 & 0 & 0 & 0 \\ 0 & \frac{2k_m l_x}{I_x} & 0 & 0 & 0 & 0 \\ 0 & 0 & \frac{2k_m l_y}{I_y} & 0 & 0 & 0 \\ 0 & 0 & 0 & \frac{4k_m}{\sqrt{2}m} & 0 & 0 \\ 0 & 0 & 0 & 0 & \frac{4k_m}{\sqrt{2}m} & 0 \\ 0 & 0 & 0 & 0 & 0 & \frac{4k_m l_z}{I_z} \end{bmatrix} \tag{2}$$

with m the MP mass, k_m the VCA motor constant, l_x, l_y and l_z the levers of torque and I_x, I_y and I_z indicating the moments of inertia in the rotational directions. Due to the neglection of cross talk, the dynamic matrix $\mathbf{A}$ has only entries in the main diagonal, representing the effective motor constants for each DoF. To transform the electrical current vector $\mathbf{i}$ into the individual currents applicable to the VCA coils $\mathbf{i_a} = \begin{bmatrix} i_1 & i_2 & i_3 & i_4 & i_5 & i_6 & i_7 & i_8 \end{bmatrix}^T$, a linear transformation $\mathbf{i_a} = \mathbf{T}\mathbf{i}$ with the transformation matrix

$$\mathbf{T} = \begin{bmatrix} \mathbf{T_{oop}} & \mathbf{0_{4,3}} \\ \mathbf{0_{4,3}} & \mathbf{T_{ip}} \end{bmatrix} = \begin{bmatrix} 1 & 1 & 0 & 0 & 0 & 0 \\ 1 & 0 & -1 & 0 & 0 & 0 \\ 1 & 0 & 1 & 0 & 0 & 0 \\ 1 & -1 & 0 & 0 & 0 & 0 \\ 0 & 0 & 0 & -1 & 1 & -1 \\ 0 & 0 & 0 & 1 & 1 & -1 \\ 0 & 0 & 0 & 1 & -1 & -1 \\ 0 & 0 & 0 & -1 & -1 & -1 \end{bmatrix} \tag{3}$$

is utilized. A nonlinear transformation

$$\boldsymbol{\zeta}_\mathbf{i} = \begin{bmatrix} \boldsymbol{\zeta}_{\mathbf{i,oop}} \\ \boldsymbol{\zeta}_{\mathbf{i,ip}} \end{bmatrix} = \mathbf{h_i}\left(\mathbf{d_i}\right) = \begin{bmatrix} \mathbf{h_{i,oop}}\left(\mathbf{d_{i,oop}}\right) \\ \mathbf{h_{i,ip}}\left(\mathbf{d_{i,ip}}\right) \end{bmatrix}, \tag{4}$$

with $\mathbf{h_i}$ being a set of trigonometric functions, is applied to transform the measured out-of-plane and in-plane distances $\mathbf{d_{i,oop}} = [d_{IPS,1}, d_{IPS,2}, d_{IPS,3}]$ and $\mathbf{d_{i,ip}} = [d_{IPS,4}, d_{IPS,5}, d_{IPS,6}]$, respectively, into the actual internal platform position $\boldsymbol{\zeta}_\mathbf{i}$.

In order to calculate the external out-of-plane position $\boldsymbol{\zeta}_{\mathbf{e,oop}}$ of the MP with respect to a sample surface using the

Post-print version of the article: D. Wertjanz, E. Csencsics, and G. Schitter, "3 DoF Vibration Compensation Platform for Robot-Based Precision Inline Measurements on Free-Form Surfaces," *IEEE Transactions on Industrial Electronics*, Early access, 2021. DOI: 10.1109/TIE.2021.3055132

three measured distances $\mathbf{d_{e,oop}} = [d_{TS,1}, d_{TS,2}, d_{TS,3}]$ by the TS, a transformation

$$\zeta_{\mathbf{e,oop}} = \mathbf{h_{e,oop}}\left(\mathbf{d_{e,oop}}\right) \tag{5}$$

as for the internal out-of-plane position is derived. Due to the placement of the three TS on the same axes as IPS_1-IPS_3 (see Fig. 2b), the internal and external out-of-plane positions show the relations

$$z_i + z_0 = -z_e \tag{6a}$$
$$\phi_{x,i} = -\phi_{x,e} \tag{6b}$$
$$\phi_{x,i} = -\phi_{y,e}, \tag{6c}$$

with z_0 being a constant offset between the measured z-position values. Considering the relations in (6), the complete model of the MP dynamics results in

$$\begin{bmatrix} \ddot{\zeta}_{\mathbf{i,oop}} \\ \ddot{\zeta}_{\mathbf{i,ip}} \end{bmatrix} = \begin{bmatrix} \mathbf{A_{oop}} & \mathbf{0_{3,3}} \\ \mathbf{0_{3,3}} & \mathbf{A_{ip}} \end{bmatrix} \begin{bmatrix} \mathbf{i_{oop}} \\ \mathbf{i_{ip}} \end{bmatrix} \tag{7a}$$
$$\begin{bmatrix} \zeta_{\mathbf{i,oop}} \\ \zeta_{\mathbf{i,ip}} \end{bmatrix} = \begin{bmatrix} \mathbf{h_{i,oop}}\left(\mathbf{d_{i,oop}}\right) \\ \mathbf{h_{i,ip}}\left(\mathbf{d_{i,ip}}\right) \end{bmatrix} \tag{7b}$$
$$\dot{\zeta}_{\mathbf{e,oop}} = \dot{\mathbf{h}}_{\mathbf{e,oop}}\left(\mathbf{d_{e,oop}}\right) = -\dot{\zeta}_{\mathbf{i,oop}}. \tag{7c}$$

IV. System Implementation and Analysis

Based on the design presented in Section II-B, the prototype of the tracking module is implemented and the real system dynamics are analyzed. Figure 3 shows a schematic system overview. Depending on the position error $\mathbf{e}_\zeta$, a reference current $\mathbf{i_r}$ is calculated. Using the transformation matrix in (3) and the gain of the analog current control k_i, the reference voltage $\mathbf{u_{a,r}}$ for the AS is calculated. Individual analog PI (proportional-integral) controllers $\mathbf{C_i}$ are used to control the eight current amplifiers $\mathbf{P_i}$. The generated currents $\mathbf{i_a}$ are applied to the VCAs. The output voltages of the IPS and TS are transformed into the measured distances $\mathbf{d_i}$ and $\mathbf{d_e}$, respectively, by use of calibrated polynomial functions. Finally, the actual internal and external position of the MP is calculated using (4) and (5). The two switches represent the control transition scheme, enabling smoothly switching between internal stabilization and external tracking, which is discussed in Section V-B.

A. Implementation of tracking module prototype

1) Mechanical structure of MP: The mechanical design of the quadratic MP is modeled with a length of 150 mm. A cross-strut is included on the bottom of the MP to achieve high stiffness and shift structural modes to higher frequencies. To keep the mass of the integrated system low, all mechanical parts, i.e. the supporting frame and the moving platform, are 3D printed using polyethylene terephthalate glycol-modified (PET-G) with a density and Young's modulus of $1.27\,\mathrm{g\,cm^{-3}}$ and 2.2 GPa, respectively, as a stiff material. The total moving mass including the mechanical structure of the MP, the coils of the VCAs and the TS is 850 g. The entirely assembled tracking module has a mass of about 4.5 kg.

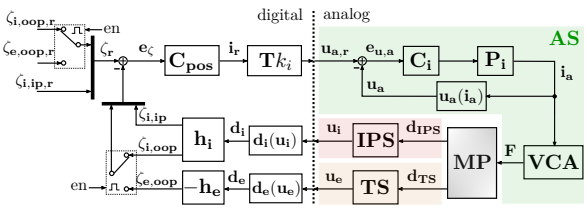

Fig. 3: Block diagram of the tracking module. The digital position control sets the reference voltage $\mathbf{u_{a,r}}$ for the individual analog current control. The force $\mathbf{F}$ generated by the VCAs is applied to the MP. The actual internal and external MP position is calculated from the distances measured by the IPS and TS.

2) Actuation system: In order to levitate and actuate the MP, conventional VCAs (VCAR0087-0062-00A, Supt-Motion, Suzhou, China) are chosen. Each VCA is capable of providing 20 N continuous force and shows a relatively large air gap of 500 µm. Considering the dynamic matrix in (2), the values of the design parameters are summarized in Tab. I. The assembled prototype achieves an actuation range of about ±180 µm and ±2 mrad in the translational and rotational DoFs. Custom-made analog proportional-integral (PI) voltage-controlled current amplifiers, based on the high-power operational amplifier OPA544T (Burr-Brown, Tucson, Arizona, United States), are utilized to apply a desired current to each coil of the VCAs. The bandwidth of each current control loop is set to 10 kHz, avoiding undesired phase lag for the subsequent position control.

TABLE I: Design parameters of the actuation system (AS).

Parameter	Value	Description
k_m	$12.7\,\mathrm{N\,A^{-1}}$	VCA motor constant
k_i	$0.4\,\mathrm{A\,V^{-1}}$	Gain of analog current control
m	850 g	Total MP mass
l_x	$\sqrt{2}$ 25 mm	Lever of torque ϕ_x
l_y	$\sqrt{2}$ 25 mm	Lever of torque ϕ_y
l_z	25 mm	Lever of torque ϕ_z
I_x	1.44 m kg	Moment of inertia ϕ_x
I_y	1.44 m kg	Moment of inertia ϕ_y
I_z	2.54 m kg	Moment of inertia ϕ_z

3) Position sensor systems:
IPS: To determine the MP's position in six DoFs with respect to the supporting frame (internal position), a custom-made IPS system based on six optical proximity sensors (HSDL-9100, Avago Technologies, San Jose, California, United States) is designed. Highly reflective tape is attached to the target points of the optical proximity sensor to achieve a high signal to noise ratio (SNR) ratio.
TS: Three capacitive displacement sensors (CSH05, Micro-Epsilon, Ortenburg, Germany) are used to measure the out-of-plane distance and orientation of the MP with respect to a sample surface (external position).

Each sensor channel of the six IPS and three TS (see Fig. 2) is calibrated using an interferometric sensor system (IDS3010, attocube - Wittenstein Group, Germany) as a reference. The

Post-print version of the article: D. Wertjanz, E. Csencsics, and G. Schitter, "3 DoF Vibration Compensation Platform for Robot-Based Precision Inline Measurements on Free-Form Surfaces," *IEEE Transactions on Industrial Electronics*, Early access, 2021. DOI: 10.1109/TIE.2021.3055132

obtained sensors characteristics are fitted by a high-order polynomial within the desired sensor range, yielding equal sensor gains. In Tab. II the noise floor and range of the two individual sensor systems are listed.

TABLE II: Parameters of IPS and TS.

Sensor	Noise floor	Range	Bandwidth
$IPS_1 - IPS_6$	75 nm rms	1.8 mm	10 kHz
$TS_1 - TS_3$	15 nm rms	0.4 mm	4 kHz

4) Rapid prototyping system: Development tools of Beckhoff Automation GmbH & Co. KG (Verl, Gütersloh, Germany) are chosen for data acquisition and rapid prototyping of the subsequent digital position control of the platform. An Ethernet/EtherCAT bus coupler (Beckhoff EK1100) is used as interface between the digital position control and the tracking module components. In order to set reference voltages for the current controllers and to read the signals of the IPS and TS, analog in- and output terminals (Beckhoff EL3702, Beckhoff EL4732) are included. The entire rapid prototyping system runs with a sampling frequency of 20 kHz and shows a time delay of about 140 µs.

B. Analysis of system dynamics

In a first step, the system dynamics are measured with a system analyzer (3562A, Hewlett-Packard, Palo Alto, CA, USA) using the signal of the IPS in a closed-loop manner. Using the system model derived in Section III and the parameters listed in Tab. I, a low-bandwidth floating-mass model-based proportional-integral-derivative (PID) controller is designed for each DoF to stabilize the levitated MP in a free-floating position with respect to its supporting frame. The analysis of the system dynamics is exemplary shown for DoF z. A sinusoidal sweep with low amplitudes (5 µm/100 µrad) is applied to the reference position of the single-input single-output (SISO) control loop. The system dynamics $G_{z,i} = \frac{z_i}{u_{z,i}}$ are obtained (see Fig. 4) by dividing the measured position z_i and the controller output $u_{z,i}$, and include the time delay of the rapid prototyping system as well as the dynamics of the AS, the MP and IPS. Due to the balanced system design, low cross talk between the DoFs is measured, which is 15 to 30 dB lower than the related system dynamics for low frequencies (data not shown). This justifies the the proposed SISO control approach.

In the frequency range below the first structural mode of the MP (< 150 Hz), the relations between the internal and external out-of-plane MP position are given by (6) and (7c), yielding equal dynamics for the internal and external position output with just opposite sign due to the equal sensor gains. Therefore, the same PID control parameters can be used for the tracking control mode by inverting the sign of the external position as indicated in Fig. 3. The identification process is repeated in closed-loop operation with the signal of the TS as feedback. As expected, similar out-of-plane dynamics as identified in the internal stabilization control mode are obtained for frequencies up to 150 Hz as shown in Fig. 4. However, due to the placement of the TS closer to the platform's center (Fig. 2b), measured structural modes of the moving platform at higher frequencies differ from the dynamics observed by the IPS. This results in different system dynamics at higher frequencies, as exemplary shown for z_i and z_e in Fig. 4 (black dashed and dotted lines). Due to the cable connection of the actuator coils mounted on the platform, parasitic stiffness and damping can be observed for frequencies lower than 25 Hz. However, between 20 and 140 Hz good agreement with the floating mass model $\frac{4k_m k_i}{ms^2}$, as modelled in (1) and (2) with the design parameters listed in Tab. I, is obtained.

V. Control Design and Implementation

A. Position control

Based on the measured system dynamics, the parameters of the SISO PID controllers

$$C_{PID} = k_p + \frac{k_i}{s} + \frac{k_d s}{1 + \frac{s}{\omega_t}} \tag{8}$$

are optimized in a loop shaping approach by following to achieve maximum bandwidth. As discussed in Section IV-B, the internal and external out-of-plane position outputs show very similar dynamics in the low frequency range. This fact enables the application of the same PID parameters for both position outputs by just inverting the sign of the external position. The parameter of the parallel tamed PID controller structure in (8) are synthesized in accord to the guidelines in [23]. With α being a tuning parameter, the P-gain $k_p = \frac{1}{\alpha}\left(|G(s)|_{s=j\omega_c}\right)^{-1}$ is used to shift the intersection of the loop gain $C_{PID}G_k$, $k \in \{i, e\}$ with the 0 dB-line to the targeted crossover frequency ω_c. The I-gain, which is active below $\frac{\omega_c}{\alpha^2}$, is used to increase the loop gain at low frequencies and thus, reduce the steady state error. The D-gain $k_d = \frac{k_p}{\alpha\omega_c}$ is required for reasons of robustness by introducing sufficient phase lead at around ω_c. A limitation of the loop gain at high frequencies is achieved by stopping the D-action with a pole at $\omega_t = \alpha\omega_c$. A reasonable value for the tuning parameter is found to be $\alpha \approx 3$ [23]. The cross-over frequencies ω_c of the designed loop gains are about 130 Hz, limited by excited structural modes and the according phase loss at higher frequencies. The controller implementation is exemplary shown for DoF z. The PID controller designed for both position outputs, z_i and z_e, is represented as solid black line in Fig. 4. However, for frequencies above 150 Hz measured structural resonances differ due to the sensor placement. Therefore, tailored notch filters for the internal and external position control are required. For the internal position (stabilization) and external position (tracking) control, two notch filters of the form

$$H_{N,k} = \frac{s^2 + \delta_k 2\pi\nu_k s + 4\pi^2\nu_k^2}{s^2 + 2\delta_k\rho_k 2\pi\nu_k s + 4\pi^2\nu_k^2},\ k \in \{1, 2\}, \tag{9}$$

with ρ_k determining the depth and δ_k the width of the notch filter at a desired frequency ν_k, are designed to attenuate occurring structural modes at higher frequencies and ensure robustness. The extended position controller is given by

$$C = C_{PID}H_{N,1}H_{N,2} = C_{PID}H_N. \tag{10}$$

Post-print version of the article: D. Wertjanz, E. Csencsics, and G. Schitter, "3 DoF Vibration Compensation Platform for Robot-Based Precision Inline Measurements on Free-Form Surfaces," *IEEE Transactions on Industrial Electronics*, Early access, 2021. DOI: 10.1109/TIE.2021.3055132

For each of the six internal and three external position outputs an individual controller is designed. The control parameters, including measured gain and phase margin of each position controller, are summarized in Tab. III.

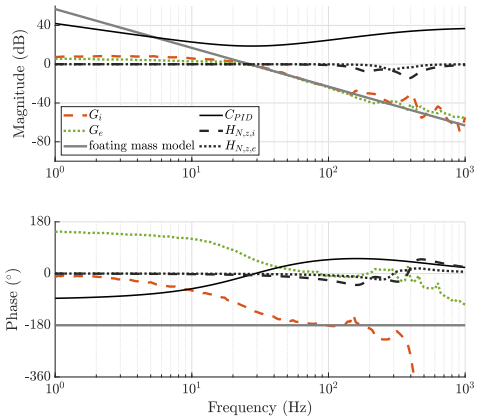

Fig. 4: System and controller dynamics of DoF z. The same PID controller (solid black) is used for the internal and external position control. Different system dynamics ($G_{z,i}$ and $G_{z,e}$) observed at higher frequencies require tailored notch filters ($H_{N,z,i}$ and $H_{N,z,e}$) for robustness.

Figure 5 shows the measured complementary sensitivity $T = \frac{C_e G_e}{1+C_e G_e}$ and sensitivity function $S = \frac{C_e}{1+C_e G_e}$ for the three external out-of-plane position outputs. The achieved position control bandwidths are between 120 to 160 Hz. Good vibration compensation capability for lower frequencies is indicated by the measured sensitivity functions S. A sinusoidal vibration with e.g. a frequency of 20 Hz can be attenuated by 15 dB, 17 dB and 20 dB in z_e, $\phi_{x,e}$ and $\phi_{y,e}$, respectively. A slight waterbed effect above the unity-gain cross-over frequency can be observed.

B. Transition scheme

For the actual operation of a robot-based inline measurement system, a robust control transition scheme between stabilization and tracking mode is required. When the robot arm is approaching a sample surface, the MP needs to maintain a constant center position with respect to its supporting frame by using the IPS in order to avoid mechanical damage. Once the TS are in range, active vibration compensation is enabled by the tracking mode, which maintains a constant displacement and orientation between the MP and the sample surface (see Fig. 1). To enable an efficient control transition between stabilization and tracking mode, a method is developed, which prevents undesired switching transients in the MP position that may damage the MT or the sample. Considering the schematic system overview in Fig. 3, the two switches are replaced by a cross-fading error gain $\gamma \in [0, 1]$. The resulting transition scheme is exemplary illustrated for DoF z in Fig. 6. The actual

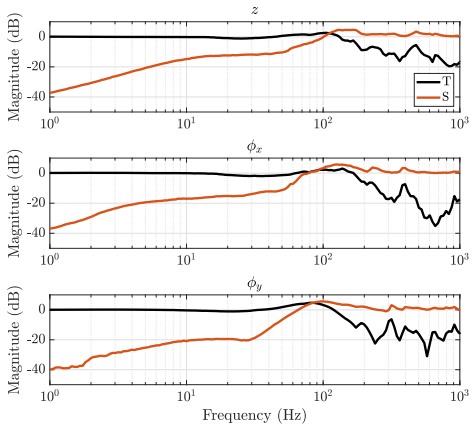

Fig. 5: Complementary sensitivity T and sensitivity function S for the external out-of-plane positions z_e, $\phi_{x,e}$ and $\phi_{y,e}$.

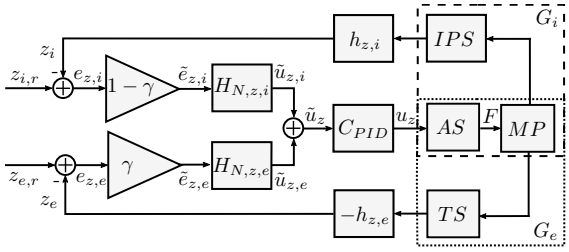

Fig. 6: An efficient transition scheme between stabilization and tracking mode of the MP using a cross-fading error gain $\gamma \in [0, 1]$ and a single PID position controller [24].

internal and external position errors $e_{z,i}$ and $e_{z,e}$ are weighted by γ and $1-\gamma$, respectively, with

$$\gamma(t) = 6\left(\frac{t}{T_t}\right)^5 - 15\left(\frac{t}{T_t}\right)^4 + 10\left(\frac{t}{T_t}\right)^3 \qquad (11)$$

following a minimum jerk trajectory in a given transition time T_t. The weighted position errors $\tilde{e}_{z,i}$ and $\tilde{e}_{z,e}$ are applied to the individual notch filters $H_{N,z,i}$ and $H_{N,z,e}$ and the sum of the notch filter outputs is applied to the PID controller C_{PID}. The transition scheme is stable for each $\gamma \in [0, 1]$ since the effective loop gain $L(\gamma) = (1-\gamma)L_i + \gamma L_e$ is a weighted superposition of the two stable loop gains $L_i = C_{PID} H_{n,z,i} G_i$ and $L_e = C_{PID} H_{n,z,e} G_e$ which have equal cross-over frequencies [24]. The tracking module is capable of performing simultaneous transitions in all three out-of-plane DoFs.

VI. Experimental Evaluation of System Performance in Vibrational Environment

In order to evaluate the vibration compensation capability of the developed tracking module as well as the performance of the control transition scheme in the three out-of-plane DoFs, a moving sample surface is required to emulate vibrations in

Post-print version of the article: D. Wertjanz, E. Csencsics, and G. Schitter, "3 DoF Vibration Compensation Platform for Robot-Based Precision Inline Measurements on Free-Form Surfaces," *IEEE Transactions on Industrial Electronics*, Early access, 2021. DOI: 10.1109/TIE.2021.3055132

TABLE III: Controller design parameters.

Output	$k_p(1)$	k_d(s/rad)	ω_t(rad/s)	k_i(rad/s)	$H_{N1}: \{\nu, \rho, \delta\}$	$H_{N2}: \{\nu, \rho, \delta\}$	GM/PM
z_i	10.54	0.034	2827.4	993.5	{190 Hz/0.5/0.3}	{389 Hz/0.2/0.5}	7 dB/24°
z_e					{290 Hz/0.55/0.25}	{400 Hz/0.8/0.2}	9 dB/34°
$\phi_{x,e}$	18.74	0.006	3298.7	2061.1	{200 Hz/0.8/0.3}	{366 Hz/0.15/0.5}	22 dB/40°
$\phi_{x,i}$					{400 Hz/0.3/0.5}	{912 Hz/0.1/0.8}	8 dB/45°
$\phi_{y,e}$	17.69	0.005	3298.7	1945.8	{180 Hz/0.7/0.2}	{500 Hz/0.5/1.8}	11 dB/36°
$\phi_{y,i}$					{400 Hz/0.3/0.5}	{794 Hz/0.5/0.3}	17 dB/35°
x	14.89	0.007	2261.9	1122.6	{200 Hz/0.8/0.6}	{400 Hz/0.5/0.6}	13 dB/53°
y	14.89	0.007	2261.9	1122.6	{200 Hz/0.8/0.6}	{470 Hz/0.5/0.6}	7 dB/52°
ϕ_z	21.03	0.009	2261.9	1558.8	{180 Hz/0.3/0.4}	{478 Hz/1/0.5}	9 dB/50°

an industrial environment. Therefore, an aluminum sample is mounted on a one DoF shaker. The entire tracking module is placed above the moving target as shown in Fig. 7, with the TS determining the actual distance and orientation between the MP and the sample surface. In DoF z a randomized vibrational disturbance according to the VC-A norm [7] is emulated by the shaker. However, non-controllable rotational motion in ϕ_x and ϕ_y occurs when actuating the shaker due to eccentric mounting of the sample.

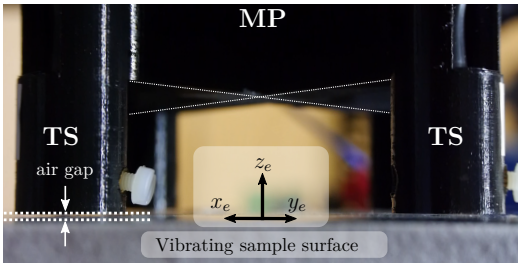

Fig. 7: Experimental setup overview. The TS are measuring the distance and orientation to the vibrating target in the DoFs z, ϕ_x and ϕ_y.

A. Control Transition

The control transition scheme is implemented for all out-of-plane DoFs and exemplary shown for DoF z in the artificially generated vibrational environment. Therefore, the platform is positioned in a free-floating position using the stabilization control mode, such that the initial external position error between the platform and a stationary sample surface is $e_{z,e,0} = 50\,\mu\text{m}$. Figure 8 shows the results related to this experiment. For $t < 0.5\,\text{s}$ the motion of the sample surface $e_{z,e} = 20.1\,\mu\text{m rms} + e_{z,e,0}$ is represented by the external error $e_{z,e}$, while the MP is stabilized with respect to the supporting frame ($e_{z,i} = 90\,\text{nm rms}$). The related control effort is represented by the current i_z applied to A_1-A_4 (see (3)) in Fig. 8c. The total force applied in direction z is $|F_z| = 4k_m i_z = 4 \cdot 12.7\,\text{N A}^{-1} \cdot 0.164\,\text{A} = 8.33\,\text{N}$, which is a reasonable value to levitate the MP with a mass of about 850 g. At $t = 0.5\,\text{s}$ the minimum jerk control transition with a transition time of $T_t = 50\,\text{ms}$ is enabled. As desired, the tracking error $e_{z,e}$ decays and, accordingly, the internal position error $e_{z,i}$ and the AC component of the control

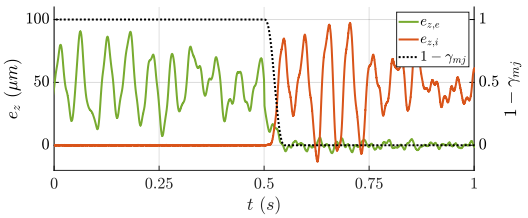

(a) Control transition in DoF z.

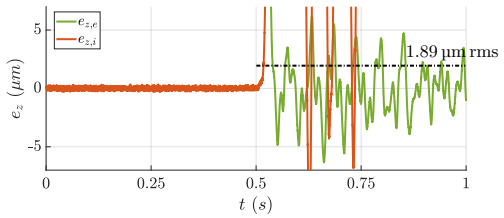

(b) Zoomed plot.

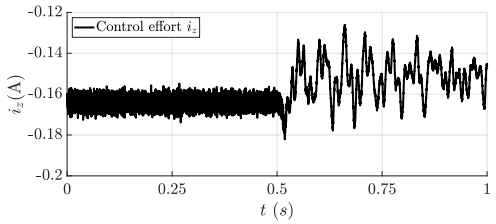

(c) Control effort.

Fig. 8: Experimental validation of the control transition scheme for DoF z. a) For $t < 0.5$ the external position error in solid black equals the sample motion. The transition is enabled at $t = 0.5\,\text{s}$. b) A residual tracking error of $e_{z,e} = 1.89\,\mu\text{m rms}$ is achieved, corresponding to a vibration attenuation of 90.4 %. c) The related control effort in A applied to each of the VCAs A_1-A_4. Follow the link https://www.acin.tuwien.ac.at/project/precision-robotic-in-line-metrology-for-freeform-surfaces to the online video.

effort increase due to the tracking motion of the platform. For $t > 0.55\,\text{s}$ a residual tracking error of $e_{z,e} = 1.89\,\mu\text{m rms}$ is achieved. Thus, the vibration disturbance in DoF z is reduced by 90.4 %.

Post-print version of the article: D. Wertjanz, E. Csencsics, and G. Schitter, "3 DoF Vibration Compensation Platform for Robot-Based Precision Inline Measurements on Free-Form Surfaces," *IEEE Transactions on Industrial Electronics*, Early access, 2021. DOI: 10.1109/TIE.2021.3055132

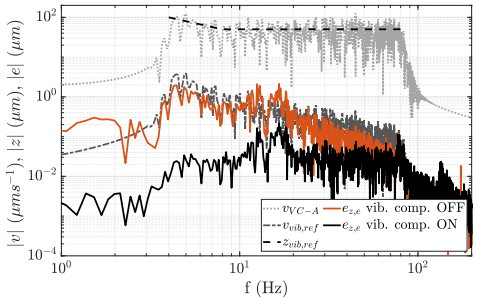

Fig. 9: Amplitude spectrum of reference (dashed-dotted grey), generated (red) and attenuated (black) vibrations. The velocity spectrum (dotted grey) of the reference accords to the VC-A standard (dotted black) [7]. Disturbance rejection better than $-20\,\mathrm{dB}$ is observed for frequencies below $40\,\mathrm{Hz}$.

B. 3 DoF vibration compensation

The vibration compensation performance in the three out-of-plane DoFs is demonstrated, again by applying a randomized z-position signal, which meets the standardized VC-A spectrum [7]. Figure 9 shows the corresponding spectrum of the reference position $z_{vib,ref}$ (dashed-dotted grey), resulting from the integration of the velocity spectrum of $v_{vib,ref}$ (dashed grey). By applying $z_{vib,ref}$ to the shaker, the tracking error $e_{z,e}$ for disabled vibration compensation in solid grey results. Repeating the measurement with enabled vibration compensation, the tracking error is significantly reduced, indicated in dashed black. Good attenuation of about $-35\,\mathrm{dB}$ for low-frequency vibrations can be observed. According to the measured sensitivity function in Fig. 5, the capability of disturbance-rejection decreases with increasing frequency of the vibrations. However, at $40\,\mathrm{Hz}$ the attenuation is still around $-20\,\mathrm{dB}$.

In Fig. 10 the according time domain signals of the out-of-plane position errors for disabled vibration compensation are shown in grey, having about $15.7\,\mu\mathrm{m\,rms}$ in z and $95\,\mu\mathrm{rad\,rms}$ in the rotational DoFs. The according peak-to-valley values are $89\,\mu\mathrm{m\,pv}$ and $740\,\mu\mathrm{rad\,pv}$. By repeating the measurement with enabled vibration compensation (black), a residual error of about $1.6\,\mu\mathrm{m\,rms}/10\,\mu\mathrm{m\,pv}$ in z_e results, which corresponds to a reduction of about $90\,\%$ for this DoF. The rotational tracking errors are reduced to about $21\,\mu\mathrm{rad\,rms}/160\,\mu\mathrm{rad\,pv}$ ($78\,\%$). The achieved system performance is orientation-independent due to the actuation principle based on identical VCAs, as demonstrated in [18].

In summary, the tracking module with integrated robust control transition scheme successfully compensates $78-90\,\%$ of disturbing vibrations in the three out-of-plane DoFs, demonstrating the feasibility and validity of the proposed system concept.

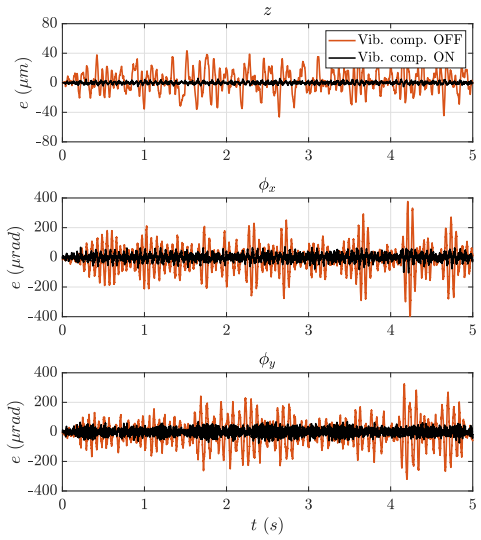

Fig. 10: Position errors for standardized floor vibrations with disabled (dotted grey) and enabled (solid black) vibration compensation. Residual rms position errors of $1.6\,\mu\mathrm{m\,rms}$ ($-90\,\%$) and $21\,\mu\mathrm{rad\,rms}$ ($-78\,\%$) are achieved for z and the rotational DoFs, respectively.

VII. Conclusion

In this paper, a three DoF MAGLEV tracking module with arbitrary operation orientation for precision robot-based surface measurements is presented. Three TS measuring the external distance and orientation relative to a sample in the three out-of-plane DoFs z, ϕ_x and ϕ_y are mounted on the MP. The implementation of SISO PID controllers enables to maintain a constant position of the MP relative to a sample surface, while the MP is stabilized in-plane with respect to the tracking module frame. The achieved position control bandwidth for each DoF is about $130\,\mathrm{Hz}$. By means of a cross-fading error gain, an effective control transition between the stabilization and tracking mode of the MP is presented and evaluated. Standardized floor vibration profiles are applied to a vibrating sample surface to evaluate the vibration compensation performance of the tracking module. Attenuation better than $-20\,\mathrm{dB}$ for frequencies below $40\,\mathrm{Hz}$ in DoF z is shown. In the time domain, a residual tracking error of about $1.6\,\mu\mathrm{m\,rms}$ is achieved for a vibration disturbance with $15.7\,\mu\mathrm{m\,rms}$, corresponding to a reduction of $90\,\%$. Angular displacements are reduced by $78\,\%$ down to $21\,\mu\mathrm{rad\,rms}$. These results clearly show the feasibility of the proposed system concept.

Next steps include the integration of in-plane TS in order to achieve vibration compensation in six DoF. Moreover, the implementation of a scanning MT will enable precision robot-based 3D measurements on free-form surfaces.

Post-print version of the article: D. Wertjanz, E. Csencsics, and G. Schitter, "3 DoF Vibration Compensation Platform for Robot-Based Precision Inline Measurements on Free-Form Surfaces," *IEEE Transactions on Industrial Electronics*, Early access, 2021. DOI: 10.1109/TIE.2021.3055132

References

[1] D. Imkamp, R. Schmitt, and J. Berthold, "Blick in die Zukunft der Fertigungsmesstechnik - Die VDI/VDE-GMA Roadmap Fertigungsmesstechnik 2020." *Technisches Messen*, vol. 10(79), 2012.

[2] T. Uhrmann, T. Matthias, M. Wimplinger, J. Burggraf, D. Burgstaller, H. Wiesbauer, and P. Lindner, "Recent progress in thin wafer processing," in *2013 IEEE International 3D Systems Integration Conference (3DIC)*, pp. 1–8, 2013.

[3] H. Schwenke, U. Neuschaefer-Rube, T. Pfeifer, and H. Kunzmann, "Optical methods for dimensional metrology in production engineering," *CIRP Annals*, vol. 51(2), pp. 685 – 699, 2002.

[4] D. J. Whitehouse, *The Handbook of Surface and Nanometrology*, 1st ed. Taylor and Francis, 2002.

[5] A. Yogeswaran and P. Payeur, "3d surface analysis for automated detection of deformations on automotive body panels," in *New Advances in Vehicular Technology and Automotive Engineering*. IntechOpen, 2012.

[6] T.-F. Yao, A. Duenner, and M. Cullinan, "In-line dimensional metrology in nanomanufacturing systems enabled by a passive semiconductor wafer alignment mechanism," *Journal of Micro- and Nano-Manufacturing*, vol. 5(1), 2016.

[7] C. G. Gordon, *Generic Vibration Criteria for Vibration-Sensitive Equipment*, Colin Gordon & Associates, 1999.

[8] R. Saathof, M. Thier, R. Hainisch, and G. Schitter, "Integrated system and control design of a one dof nano-metrology platform," *Mechatronics*, vol. 47, pp. 88 – 96, 2017.

[9] J. van Eijk, D. Laro, J. Eisinger, W. Aarden, T. Michielsen, and S. van den Berg, "The "ultimate performance" in floor vibration isolation," *Mikroniek. Professional Journal on Precision Engineering*, vol. 51, pp. 13–19, 2011.

[10] E. Savio, L. D. Chiffre, and R. Schmitt, "Metrology of freeform shaped parts," *CIRP Annals*, vol. 56, no. 2, pp. 810 – 835, 2007.

[11] J. Rejc, J. Cinkelj, and M. Munih, "Dimensional measurements of a gray-iron object using a robot and a laser displacement sensor," *Robotics and Computer-Integrated Manufacturing*, vol. 25(1), pp. 155–167, 2009.

[12] U. Schneider, J. R. D. Posada, M. Drust, and A. Verl, "Position control of an industrial robot using an optical measurement system for machining purposes," *Proceedings of the 11th International Conference on Manufacturing Research (ICMR2013), Cranfield, UK*, 2013.

[13] S. Ito, D. Neyer, S. Pirker, J. Steininger, and G. Schitter, "Atomic force microscopy using voice coil actuators for vibration isolation," *2015 IEEE International Conference on Advanced Intelligent Mechatronics (AIM)*, pp. 470–475, 2015.

[14] M. Thier, R. Saathof, R. Hainisch, and G. Schitter, "Vibration compensation platform for robot-based nanoscale measurements." *15th International Conference of the EUSPE*, pp. 59–71, 2015.

[15] M. Thier, R. Saathof, E. Csencsics, R. Hainisch, A. Sinn, and G. Schitter, "Design and control of a positioning system for robot-based nanometrology." *at- Automatisierungstechnik*, vol. 63, pp. 727 – 738, 2015.

[16] R. Deng, R. Saathof, J. Spronck, S. Hol, and R. H. Munnig Schmidt, "Integrated 6-dof lorentz actuator with gravity compensator for precision positioning." *22nd International Conference on Magnetically Levitated Systems and Linear Drives (MAGLEV)*, 2014.

[17] M. Thier, R. Hainisch, G. Schitter, and R. Saathof, "Metrology platform to enable in-line nanometrology," *Industrial Technologies, Amsterdam, The Netherlands*, 2016.

[18] D. Wertjanz, E. Csencsics, J. Schlarp, and G. Schitter, "Design and control of a maglev platform for positioning in arbitrary orientations," in *2020 IEEE/ASME International Conference on Advanced Intelligent Mechatronics (AIM)*, pp. 1935–1942, 2020.

[19] J. Schlarp, E. Csencsics, and G. Schitter, "Optical scanning of a laser triangulation sensor for 3-d imaging," *IEEE Transactions on Instrumentation and Measurement*, vol. 69(6), pp. 3606–3613, 2020.

[20] P. Pavlicek and E. Mikeska, "White-light interferometer without mechanical scanning," *Optics and Lasers in Engineering*, vol. 124, p. 105800, 01 2020.

[21] R. M. Schmidt, G. Schitter, A. Rankers, and J. van Eijk, *The Design of High Performance Mechatronics*, 2nd ed. IOS Press, Amsterdam, 2014.

[22] S. Kang, M. G. Lee, and Y. Choi, "Six degrees-of-freedom direct-driven nanopositioning stage using crab-leg flexures," *IEEE/ASME Transactions on Mechatronics*, vol. 25, no. 2, pp. 513–525, 2020.

[23] E. Csencsics and G. Schitter, "Parametric pid controller tuning for a fast steering mirror," in *2017 IEEE Conference on Control Technology and Applications (CCTA)*, pp. 1673–1678, 2017.

[24] D. Wertjanz, E. Csencsics, and G. Schitter, "An efficient control transition scheme between stabilization and tracking task of a maglev platform enabling active vibration compensation," in *2020 IEEE/ASME International Conference on Advanced Intelligent Mechatronics (AIM)*, pp. 1943–1948, 2020.

Daniel Wertjanz is doctoral researcher at the Automation and Control Institute (ACIN) at TU Wien, Vienna, Austria. He received an MSc. degree in Electrical Engineering from TU Wien in 2019. His primary research interests are on high performance mechatronic systems design, high precision motion control, and automated inline measurement systems.

Ernst Csencsics is postdoctoral researcher in the Advanced Mechatronic Systems Lab at the Automation and Control Institute (ACIN) of TU Wien. He received an M.Sc. and a Ph.D. degree (sub auspiciis) in Electrical Engineering from TU Vienna, Austria in 2014 and 2017, respectively. His primary research interests are on high performance mechatronic systems, the development of holistic methods for multidisciplinary system design and integration, opto-mechatronic measurement and imaging systems, precision engineering, and robot-based in-line measurement systems. He received the journal best paper award of IEEE/ASME Transactions on Mechatronics (2018) and the best student paper award at the American Control Conference (2016).

Georg Schitter is Professor for Advanced Mechatronic Systems at the Automation and Control Institute (ACIN) of TU Wien. He received an MSc in Electrical Engineering from TU Graz, Austria (2000) and an MSc and PhD degree from ETH Zurich, Switzerland (2004). His primary research interests are on high-performance mechatronic systems, particularly for applications in the high-tech industry, scientific instrumentation, and mechatronic imaging systems, such as AFM, scanning laser and LIDAR systems, telescope systems, adaptive optics, and lithography systems for semiconductor industry. He received the journal best paper award of IEEE/ASME Transactions on Mechatronics (2018), of the IFAC Mechatronics (2008-2010), of the Asian Journal of Control (2004-2005), and the 2013 IFAC Mechatronics Young Researcher Award. He served as an Associate Editor for IFAC Mechatronics, Control Engineering Practice, and for the IEEE Transactions on Mechatronics.

Post-print version of the article: D. Wertjanz, E. Csencsics, and G. Schitter, "3 DoF Vibration Compensation Platform for Robot-Based Precision Inline Measurements on Free-Form Surfaces," *IEEE Transactions on Industrial Electronics*, Early access, 2021. DOI: 10.1109/TIE.2021.3055132